Pergamon

Int. J. Heat Mass Transfer. Vol. 39, No. 8, pp. 1617–1624, 1996

0017–9310/96 $15.00+0.00

0017–9310(95)00262–6

Effect of valve lift and disk surface on two-phase critical flow at hot water relief valve

MASAHIRO OSAKABE and MASAHIKO ISONO

Tokyo University of Mercantile Marine, 2-1-6 Etchujima Koutou-ku, Tokyo 135, Japan

(*Received* 9 *January* 1995 *and in final form* 4 *July* 1995)

Abstract—Critical flows through disk-type relief valves with different disk surfaces and lifts were investigated experimentally. The disk surfaces used were fouling brass with calcium scale, mirror-finished brass and clean Teflon. The critical flow rate obtained from the experiment was sufficiently higher than that calculated by the empirical correlation which is often used for calculation of valve capacity. From the comparison with data and a nonequilibrium homogeneous model, nonequilibrium effect was smallest in a valve using a disk of fouling brass and highest in a valve using a disk of mirror-finished brass. The nonequilibrium state was affected with flashing characteristics of valve disks and effects of lift were relatively small.

1. INTRODUCTION

Industrial plants for power generation or chemical production are frequently operated employing high pressure vessels. Maximum operating pressure in the vessels must not be exceeded for safety. If the pressure rises above the maximum pressure, pressure relief valves or safety valves are used to depressurize the vessels. However, the depressurization rate is limited by critical flow rates through the valves. So predictions of the critical flow rates through the valves are very important for design of industrial high pressure vessels.

Many studies have been conducted to clarify the two-phase critical flow for various geometrical and thermodynamic parameters [1]. Several critical flow models have been successful in describing two-phase flashing flow in well-defined nozzles and short tubes. However the applicability of these models to pressure relief valve geometry is not completely resolved [2]. The thermodynamic nonequilibrium state affected by the geometry is not clear.

In the regulation of boiler and pressure vessel in Japan, an empirical correlation is recommended to estimate the critical flow rate through the valves [3]. The correlation has been proposed by Brocket and King [4], which includes a empirical constant κ depending on the valve inlet subcooling. On the other hand, the flashing flow rate through an orifice can be described with the critical flow rate only at high pressures and relatively large flow contraction ratio [5]. When the contraction ratio is small enough, flow rate through orifice agrees well with Bernoulli equation for single water flow [6]. As the critical condition in a valve or an orifice strongly depends on the nonequilibrium factor, the observed phenomena becomes so complicated.

The most popular and pioneering model to describe the critical two-phase flow at an abrupt flow contraction such as a valve or an orifice is the nonequilibrium homogeneous model by Henry and Fauske [7]. In the model, the critical flow rate can be obtained from the energy equation frozen at the inlet quality and the equation for the sonic velocity taking into account the nonequilibrium effect. The intersecting point of the two equations is not always coincident with the maximum flow rate predicted by the energy equation [8]. Furthermore the energy equation becomes the Bernoulli equation and does not have a maximum at the inlet subcooling condition. So the model is useful for the rough calculation of the critical flow rate but is difficult to consider the intersecting point as the physically correct critical point. In the present study, a homogeneous model [8–10] based on the isentropic equation of state was modified to express the nonequilibrium effect. In the model, the quality in the energy equation is not frozen and the intersecting point of the two equations is always coincident with the maximum of the flow rate whenever the maximum exists. The direct usage of the state equation describing the nonequilibrium state provides an easy approach to clarify the nonequilibrium effect and makes clear the two mechanisms employed to reach the critical condition.

Typical pressure relief valves used in recent boilers are disk-type relief valves and are different from globe-type valves used in the experiment by Brocket and King. Nowadays disk-type relief valves are used worldwide to avoid a sticking accident of valves. In these valves, a disk of new materials such as Teflon instead of metal is sometimes used to reduce the leak flow at the closed position. Discharge experiments of subcooled water from a disk-type relief valve of different disk surfaces and lifts were conducted to

NOMENCLATURE

A	curtain area
C_P	specific heat
d	bore diameter
d_1	diameter of orifice hole
d_0	pipe diameter
G	mass velocity
G^*	nondimensional mass velocity $(=G/(P_0/V_{L0})^{1/2})$
g	acceleration due to gravity
H_{LG}	latent heat
L	valve lift
N	nonequilibrium factor
P	pressure
P_s	saturation pressure
T	temperature
V	specific volume
V_{LG}	specific volume different between water and steam.

Greek symbols

α	vena contraction coefficient at throat (valve coefficient)
β	flow area contraction ratio of orifice $(=(d_1/d_0)^2)$
η_t	nondimensional pressure ratio at throat $(=P_t/P_0)$
η_s	nondimensional saturation pressure ratio $(=P_s/P_0)$
κ	empirical constant in Brocket and King correlation.

Subscripts

C	critical
G	gas phase
L	liquid phase
s	saturation
t	throat
0	inlet.

verify the empirical correlation by Brocket and King and to understand the nonequilibrium phenomenon in the valves. Mechanism of critical flow in the valve was discussed comparing the experimental results with the proposed nonequilibrium model. Nonequilibrium factors in the valve of different disk surfaces and lifts were determined and factors affecting the nonequilibrium state were considered.

2. NONEQUILIBRIUM HOMOGENEOUS MODEL

A schematic flow pattern through valve throat is shown in Fig. 1. Fluid at a pressure of P_0 is depressurized to a pressure P_1 due to the contraction at the valve throat. The minimum flow area is the curtain area, $A = \pi dL$, at the valve seat. The maximum velocity is achieved at the actual throat slightly outside of the minimum flow area such as in an orifice. The pressure at the throat is defined as P_t. As the flow contraction and flashing takes place rapidly, it is considered that the generated bubble diameter is so small that the velocity difference between bubbles and water can be negligible. Though the bubble population density is considered to be higher near the disk surface, the homogeneous two-phase critical flow is assumed to obtain a simple model. From the energy equation, the mass velocity at the valve throat is

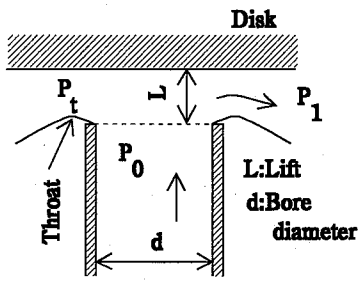

Fig. 1. Flow contraction of disk-type valve.

$$G_t = \left[-2\int_{P_0}^{P_t} V\,dP\right]^{1/2} \Big/ V_t. \tag{1}$$

At the inlet subcooling condition, the integration of equation (1) is partitioned into two parts with the saturation pressure P_s corresponding to the inlet water temperature T_0.

$$G_t^2/2 = \left[-\int_{P_0}^{P_s} V_{L0}\,dP - \int_{P_s}^{P_t} V\,dP\right] \Big/ V_t^2. \tag{2}$$

By treating the water below the pressure P_s as an incompressible fluid, V_{L0} in the first term of the right-hand side of equation (2) is constant, thus;

$$G_t^2/2 = \left[-V_{L0}(P_s - P_0) - \int_{P_s}^{P_t} V\,dP\right] \Big/ V_t^2. \tag{3}$$

The depressurization below the pressure P_s results as the rapid expansion of fluids due to the steam generation. To describe such an isentropic change of state, the following model by Epstein *et al.* [9] is employed.

$$\frac{V}{V_{L0}} = \omega\left[\frac{P_s}{P} - 1\right] + 1 \tag{4}$$

where ω is constant and is given by Leung *et al.* [10] as

$$\omega = \frac{C_{P0} T_0 P_s}{V_{L0}} \left[\frac{V_{LG0}}{H_{LG0}} \right]^2. \quad (5)$$

In equation (5), all physical properties are to be evaluated at the saturation condition corresponding to the inlet water temperature T_0. This equation for the state change is very good approximation near the saturation condition and agrees well with those obtained from the steam table within the present experimental range. The nonequilibrium state is considered to be the state where the steam generation and the isentropic expansion described by equation (4) is depressed due to the rapid flow contraction. To describe such a nonequilibrium state, equation (4) is modified with the nonequilibrium factor N to the following equation.

$$\frac{V}{V_{L0}} = N\omega \left[\frac{P_s}{P} - 1 \right] + 1. \quad (6)$$

The nonequilibrium factor N is unity in the equilibrium state and zero in the perfect nonequilibrium state. When N is small, the change of the specific volume due to the depressurization is small. The specific volume is held at V_{L0} of the saturated liquid at the pressure P_s when N is zero. When equation (6) is substituted into equation (3),

$$(G_t V_t)^2/2 = V_{L0}(P_0 - P_s) + V_{L0}[N\omega P_s \ln(P_s/P_t) - (N\omega - 1)(P_s - P_t)]. \quad (7)$$

When the nondimensional expression of

$$\eta_t = P_t/P_0$$
$$\eta_s = P_s/P_0$$
$$G_t^* = G_t/[P_0/V_{L0}]^{1/2}$$

is defined, equation (7) becomes;

$$G_t^* = [2(1-\eta_s) + 2N\omega\eta_s \ln(\eta_s/\eta_t) - 2(N\omega - 1)(\eta_s - \eta_t)]^{1/2}/[N\omega(\eta_s/\eta_t - 1) + 1]. \quad (8)$$

When $\eta_t > \eta_s$, equation (3) directly gives;

$$G_t^* = [2(1-\eta_t)]^{1/2}. \quad (9)$$

Equation (9) is also derived from the Bernoulli equation for the single-phase flow.

In the critical flow, concept of the sonic velocity is very important. When flow velocity becomes the sonic velocity, the pressure in the downstream can not transmit to the upstream and the flow rate is limited at the sonic velocity. The mass velocity corresponding to the sonic velocity is expressed as;

$$G_t = \left[-\frac{dV}{dP} \right]_t^{-1/2}. \quad (10)$$

By differentiating equation (6)

$$\frac{dV}{V_{L0}} = -N\omega P_s \frac{dP}{P^2}. \quad (11)$$

From equations (10) and (11),

$$G_t = \left[\frac{N\omega P_s V_{L0}}{P_t^2} \right]^{-1/2}. \quad (12)$$

By using nondimensional parameter

$$G_t^* = \eta_t [N\omega\eta_s]^{-1/2}. \quad (13)$$

Equation (13) is applicable when the pressure falls below the saturation pressure and the flashing takes place. In general case when the flashing does not take place, the sonic velocity in water is higher than the water velocity in the valve and the critical condition limited with the sonic velocity does not take place. For a two-phase flow, the mass velocity equation (8) does not always have the maximum point. Whenever the maximum point exists, sonic velocity equation (13) intersects at the point.

The relationship of G_t^* and η_t when the nonequilibrium parameter N is 1 is shown in Fig. 2. The model prediction is performed at the different inlet subcooling under the inlet pressure P_0 of 0.69 MPa. The solid line is calculated with the mass velocity equation (8) at $\eta_t < \eta_s$ and Bernoulli equation (9) at $\eta_t > \eta_s$. The broken line shows the sonic mass velocity equation (13). When the inlet subcooling is 0 K, equa-

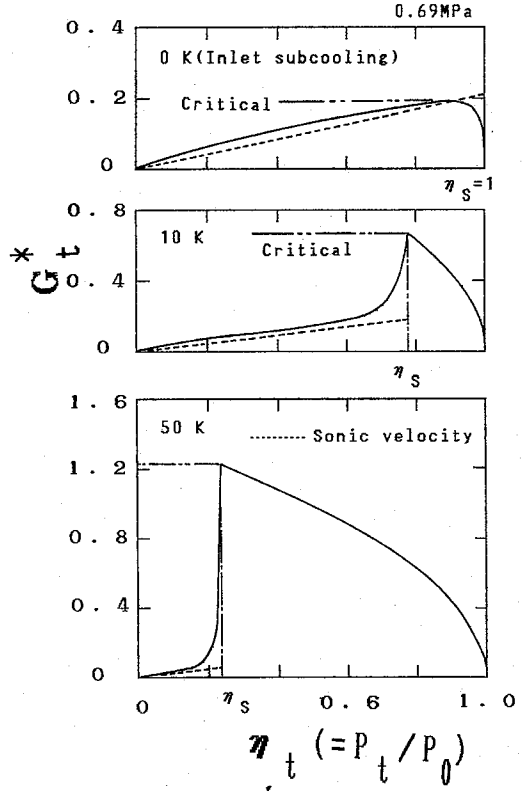

Fig. 2. Relation of nondimensional mass velocity and pressure ratio at different subcooling.

tion (8) has the maximum points where the sonic equation intersects. So by reducing η_t from 1, the mass velocity increases up to the maximum value and holds the value corresponding to the critical condition. Reducing η_t at the inlet subcooling of 10 and 50 K, the mass velocity increases upto the maximum value at η_s which already exceeds the sonic velocity. When the flashing takes place at η_s, the single-phase flow changes to the two-phase flow accompanied with the reduction of the sonic velocity. So at the flashing inception, the subsonic velocity under the single-phase suddenly becomes the supersonic velocity under the two-phase flow. It is very interesting that equation (8) at $\eta_t < \eta_s$ does not have the maximum points intersecting with the sonic velocity but the critical condition is attained at η_s and described with Bernoulli equation (9). This indicates the critical condition is obtained at the saturation pressure at the valve throat where the flashing inception takes place. In the single-phase compressible fluid, the critical condition always coincides with the sonic velocity condition. But in the two-phase flow, the critical condition does not always coincide with the sonic velocity condition.

The model prediction at the different non-equilibrium parameter N under the subcooling of 10 K is shown in Fig. 3. By reducing N, prediction with the mass velocity equation (8) at $\eta_t < \eta_s$ changes to convex curve having the maximum value from the concave one. The critical condition is obtained at η_s when the maximum value is not calculated with equation (8). The maximum value described with equation (8) is the critical condition corresponding to the sonic velocity condition. As the parameter N is smaller and the nonequilibrium is stronger, the larger critical mass velocity is predicted at the smaller η_t. When $N = 0.067$, the maximum of equation (8) takes place at η_s, which is the boundary between the two regions. One is the region where the critical flow rate is described with the Bernoulli equation (9) using the saturation pressure at the valve throat corresponding to the inlet water temperature, and the other is the region described with the maximum of equation (8). At the perfect nonequilibrium state of $N = 0$, the mass velocity equation becomes the Bernoulli equation which does not have the maximum value and the sonic velocity equation (13) which becomes the vertical line at $\eta_t = 0$ has no intersection with the Bernoulli equation. At $N = 0$ the mass velocity simply increases by reducing η_t following on the Bernoulli equation.

The comparison of the present model with Ogasawara's experimental data [5] for flashing flow of saturated liquid through orifices at inlet pressure of 4.3–4.8 MPa, is shown in Fig. 4. The solid lines show the present model and the broken line shows the critical flow rate. As the smaller flow area contraction ratio β, the experimental data agree with the model of the smaller nonequilibrium factor N indicating the stronger nonequilibrium effect. When the contraction ratio is small enough, such as $\beta = 6.2 \times 10^{-3}$, the flow rate from the orifice can be described well with the

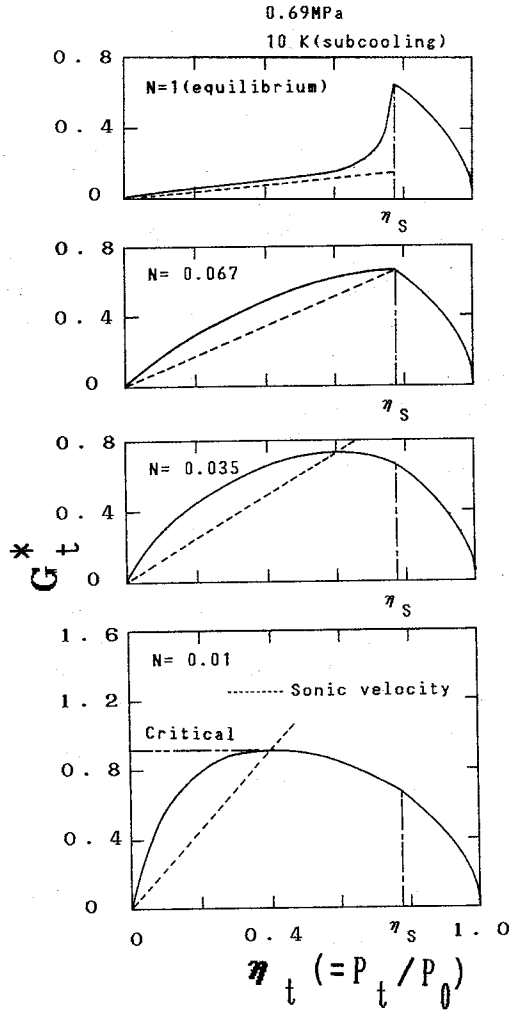

Fig. 3. Relation of nondimensional mass velocity and pressure ratio at different nonequilibrium factor.

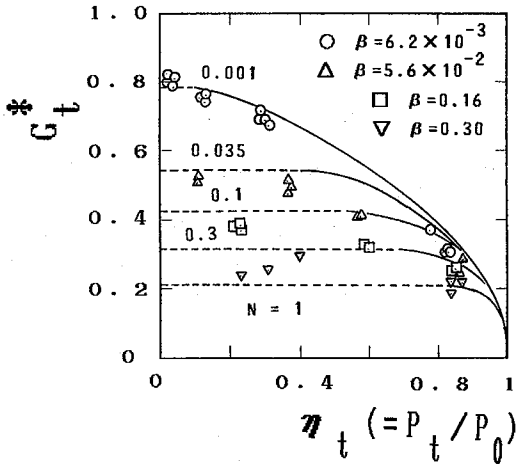

Fig. 4. Model comparison with data of orifice flashing flow by Ogasawara.

model of $N = 0.001$, which is approximately the same as the Bernoulli equation for single-phase water flow. It is clear that the flow contraction ratio is the important parameter dominating the nonequilibrium behavior of orifice flow.

3. NONEQUILIBRIUM CRITICAL FLOW MODEL

The above discussion showed that the critical flow rate can be described with either the Bernoulli equation (9) with the saturation pressure at the throat or the maximum value in the mass velocity equation (8). As $dG_t^*/d\eta_t$ is 0 at the maximum value in equation (8),

$$[N\omega+1/(N\omega)-2][\eta_c^2/(2\eta_s)]-2(N\omega-1)\eta_C + N\omega\eta_s \ln(\eta_C/\eta_s)+1.5N\omega\eta_s-1=0 \quad (14)$$

where η_C is the pressure ratio at the critical condition. From equation (14), η_C can be obtained with trial-and-error procedure at the given N, ω and η_s. The critical mass velocity is obtained with the sonic velocity equation (13) by using η_C as

$$G_C^* = \eta_C[N\omega\eta_s]^{-1/2}. \quad (15)$$

When the critical velocity is expressed with the Bernoulli equation (9)

$$G_C^* = [2(1-\eta_s)]^{1/2}. \quad (16)$$

At the boundary of the above two equations, the mass velocities with equations (15) and (16) must be the same and η_s is equal to η_C, as in the case of $N = 0.067$ in Fig. 3. By setting $\eta_s = \eta_C$ and deleting G_C^* in equations (15) and (16):

$$\eta_s = 2N\omega/(2N\omega+1) \quad (17)$$

where η_s and ω are dependent on the inlet pressure and subcooling. So equation (17) gives the relation among the inlet pressure, subcooling and nonequilibrium parameter N at the boundary condition.

The boundary calculated with equation (17) at pressure of 8–0.1 MPa is shown in Fig. 5 as a function of the nonequilibrium parameter N and the inlet subcooling ΔT_{SUB}. The right-hand side of each curve is the high subcooling region where the critical mass velocity is expressed with the Bernoulli equation (9). The left-hand side of the curves is the low subcooling region where the critical mass velocity is expressed with the maximum of the mass velocity equation and is calculated with equations (14) and (15). As the nonequilibrium is smaller (N is larger), the region described with the Bernoulli equation becomes larger.

4. EXPERIMENTAL APPARATUS AND PROCEDURE

The schematic of the experimental apparatus is shown in Fig. 6. The apparatus consisted of the pressure vessel of 0.596 m^3, steam supply line from a cylindrical main boiler, and the discharge line of 25.4 mm diameter. The main boiler had steam and water volumes of 5.4 and 1.62 m^3, respectively, and enabled the steady state experiments keeping a constant pressure at the valve inlet. The electric pressure gauges and T-type thermocouples were installed as shown in the figure. The vortex-shedding flow meter was installed at the upstream of the test section. The flow in the flow meter was considered to be single phase. The detecting unit in the flow meter was a piezoelectric device to count the vortex-shedding period. The measuring range was 1.36×10^{-3} to 8.33×10^{-5} m^3 s^{-1} and the error was $\pm1\%$ of the maximum span. To control the pressure drop in the test valve, a control valve was installed in the downstream of the test valve. The two-phase flow after the control valve was released into the atmosphere.

The cross-section of the relief valve tested is shown in Fig. 7. The lift adjusting mechanism was installed in an industrial disk-type valve of 1 inch nominal size. In the present experiment, the valve lifts were set at 0.65, 0.8 and 1.0 mm. The standard lift for an industrial usage is 0.8 mm. In the present experimental range, the valve belongs to the low-lift-type because the lift to seat diameter ratio L/d is 0.026–0.04. In a

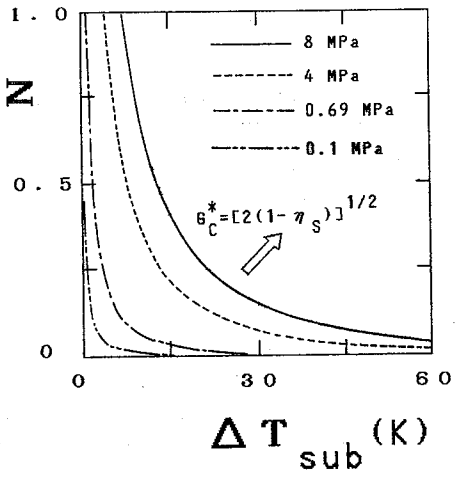

Fig. 5. Boundary of two regions for critical flow calculation.

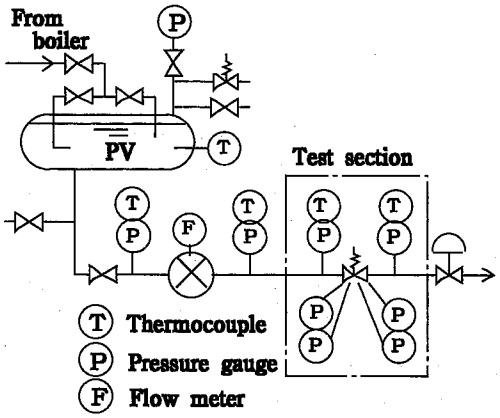

Fig. 6. Schematics of experimental apparatus.

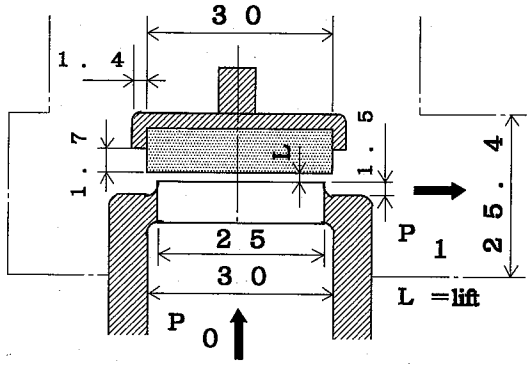

Fig. 7. Cross-section of test valve.

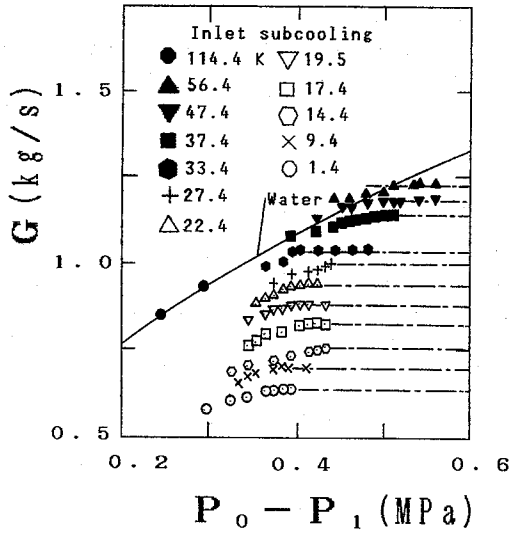

Fig. 8. Experimental result for valve with fouling disk.

low-lift-type valve, the flow area is the minimum at the curtain area of $A = \pi dL$.

Three kinds of valve disk, fouling brass with calcium scale, mirror-finished clean brass and clean Teflon, were used to clarify the disk surface effect on the flashing. The fouling disk with the calcium scale spots was obtained by flashing experiments using tap water for several months. The experiment using the fouling disk is especially important for the low pressure relief valve such as used in a low pressure boiler using tap water.

Before the experiment, a tap water or an ion-exchanged water of 0.4 m^3 hold in the pressure vessel were heated up and degassed gradually by injection of the high temperature steam from the main boiler. A tap water was used for experiments using the fouling valve and an ion-exchanged water was used for the other experiments. When the desired pressure and the temperature was achieved, hot water was released from the test valve. The valve between the main boiler and the pressure vessel was kept being opened to hold a constant pressure at the valve inlet during the experiment. The valve inlet subcooling was maintained at a constant value and the valve outlet pressure was controlled with the control valve in the downstream of the test valve. The range of inlet pressure was 0.63–0.74 MPa and the inlet subcooling was 1–59 K in the present experiments.

5. EXPERIMENTAL RESULTS AND DISCUSSION

The relation between the valve pressure difference $P_0 - P_1$ and the mass flow rate G through the fouling valve at different inlet subcoolings under the pressure of 0.69 MPa is shown in Fig. 8. The pressure difference was obtained from the pressures measured at approximately 5 cm upstream and downstream from the minimum flow area in the valve. The data at subcooling of 114.4 K was obtained at the nonflashing condition in the valve. The solid line is the following Bernoulli equation describing the single-phase flow and agrees well with the nonflashing data.

$$G = \alpha A[2(P_0 - P_1)/V_{L0}]^{1/2} \tag{18}$$

where α is the valve coefficient and measured as $\alpha = 0.615$ by using water, which agrees well with the recommended value by the valve vendor. As the pressure drop in the valve mainly depends on the flow contraction in the valve, the valve coefficient is considered to be vena contraction coefficients as same as an orifice. The curtain area A at the standard lift of 0.8 mm is $25\pi \times 0.8 = 62.83$ mm^2. When the inlet subcooling is not so high and the flashing in the valve takes place, Fig. 8 shows the critical condition where the mass flow rate G does not increase even when the pressure difference through the valve is increased. One-dot-dashed line in the figure shows the recognized critical flow rate.

For the critical flow rate in the relief valve, Brocket and King [4] conducted the hot water relief experiment by using a globe-type valve at different subcoolings under the pressure of 0.35–0.69 MPa. From the experimental results, the following empirical correlation for the nondimensional mass velocity G_C^* was proposed.

$$G_C^* = \alpha[2\kappa]^{1/2} \tag{19}$$

where κ is the empirical constant and is given as a curve depending on the inlet subcooling ΔT_{SUB}. When the least squares method is applied to the curve at $0 \leqslant \Delta T_{SUB} \leqslant 60$ K,

$$\kappa = 0.0707 + 0.0157\,\Delta T_{SUB} - 1.26 \times 10^{-4}\,\Delta T_{SUB}^2 + 3.92 \times 10^{-7}\,\Delta T_{SUB}^3. \tag{20}$$

The error due to the approximation to obtain equation (20) is within $\pm 1\%$.

Recently Sallet [11] conducted the critical flow experiment by using the disk-type relief valve such as used in the present experiment at different subcoolings under the pressure of 0.41–0.69 MPa. The experimental data agreed well with the following empirical correlation.

$$G_C^* = \alpha[2(1-0.75\eta_s)]^{1/2}. \quad (21)$$

It was reported that the effects of the nozzle shapes and the surface roughness in the upstream of the valve throat were small.

When the present nonequilibrium model is applied to the valve of the vena contraction factor α,

(i) for $\eta_s \geqslant 2N\omega/(2N\omega+1)$

$$G_C^* = \alpha\eta_C[N\omega\eta_s]^{-1/2} \quad (22)$$

where η_C is obtained from equation (14) and

(ii) for $\eta_s \leqslant 2N\omega/(2N\omega+1)$

$$G_C^* = \alpha[2(1-\eta_s)]^{1/2}. \quad (23)$$

The critical mass velocity obtained in the valves using the different disk surfaces is compared to the empirical correlations and the non-equilibrium model. The relationship of the nondimensional mass velocity and the valve inlet subcooling at the standard lift of 0.8 mm is shown in Fig. 9. The experimental mass velocity is sufficiently higher than the empirical correlation by Brocket and King which is used to determine the capacity of valve in Japan. The solid curves show the nonequilibrium model at the nonequilibrium factor N of 0.004, 0.01, 0.035 and 1. The curves of the different N merge in the equilibrium curve of $N = 1$ with increasing the valve inlet subcooling. From the comparison with the data and the model, the non-equilibrium factor N is highest in the valve using the fouling brass and smallest in the valve using the mirror-finished clean brass. It is considered that the nonequilibrium state is affected with the flashing characteristics of the valve disks. The porous structure such as in the calcium scale or the Teflon provides the more amount of cavities for the nucleations of bubbles. It should be noted that the nonequilibrium effect on the critical mass velocity appears strongly at relatively low inlet subcooling region both in the model and the experimental results.

Young and Hummel [12] enhanced the bubbling behavior and the nucleate boiling heat transfer by adding spots of Teflon either on the heated surface or in pits on the surface. The enhancement is associated with the fact that the crevices of the Teflon spots provide sufficient numbers of active sites for bubble nucleation. In their experiment nucleation could be initiated at very low superheat levels at the surface with Teflon spots. Also in the boiling heat transfer experiment by Isono [13], the more violent bubbling behavior is observed on the fouling copper surface with the calcium scale spots compared to that on the clean mirror-finished surface at the same heat flux condition. It is considered that the fouling disk with calcium scale spots provides the same low non-equilibrium state as the surface with the Teflon spots.

The comparison at the different lift of 0.65, 0.8 and 1.0 mm for the valve using the disk of clean Teflon is shown in Fig. 10. The experimental data agree well with the model of $N = 0.01$ and the effect of the lift is small. Figure 11 shows the same comparison for the valve using the disk of mirror-finished clean brass. A smaller value for N is estimated with the smaller lift but the difference is relatively small compared to the scattering of data.

6. CONCLUSION

The hot water relief experiments were performed by using a valve of different disk surfaces and different lifts. The experimental data were compared with empirical correlations and a nonequilibrium homogeneous model. The following major results were obtained:

(1) A nonequilibrium homogeneous model based on the isentropic equation of state was proposed. The direct usage of the state equation describing non-equilibrium provided the easy approach to clarify the nonequilibrium effect and made clear the two different regions. One is the region where the critical flow rate is

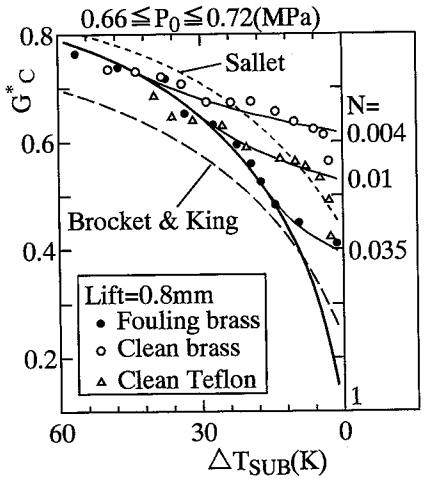

Fig. 9. Nonequilibrium affected with disk surfaces.

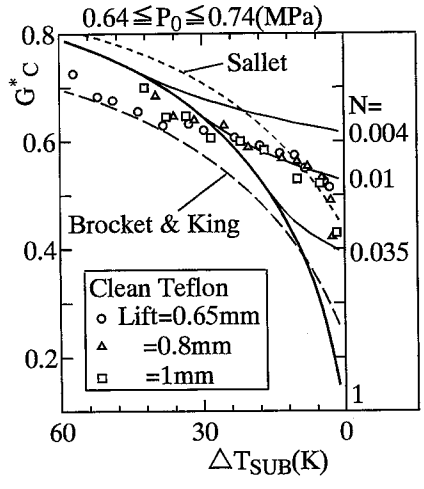

Fig. 10. Effect of lift for valve with disk of clean Teflon.

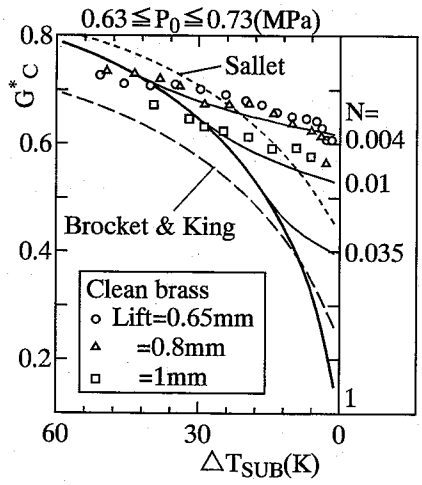

Fig. 11. Effect of lift for valve with disk of clean mirror-finished brass.

described with the Bernoulli equation using saturation pressure at the valve throat corresponding to the inlet water temperature, and the other is the region described with the maximum of the energy equation.

(2) The experimental mass velocity was sufficiently higher than that calculated from the empirical correlation by Brocket and King which is used to determine the valve capacity. From a comparison between the experimental data and the predictions with the proposed nonequilibrium model, the nonequilibrium factor N became highest in the valve with the disk of fouling brass and smallest in the valve with the disk of mirror-finished clean brass. It was considered that the nonequilibrium state was affected by flashing characteristics of the valve disk surfaces, and that the effect of the lift on the nonequilibrium state was relatively small.

(3) The nonequilibrium effects on the critical flow rate appeared strongly at relatively low inlet subcooling conditions both in the experimental data and predictions with the nonequilibrium model.

REFERENCES

1. F. Hardekopf and D. Mewes, The pressure ratio of critical flows, *Chem. Engng Technol.* **12,** 89–96 (1989).
2. J. E. Huff, Multiphase flashing flow in pressure relief systems, *Plant/Opns Prog.* **4**(4), 191–199 (1985).
3. T. Kubo, Relief valves sizing for hot water by Appurtenances Committee of the Japan Boiler Association, *Boiler Res.* 240 (April) (1990) [in Japanese].
4. G. F. Brocket and C. F. King, Sizing control valves handling flashing liquids, *Instruments* **26,** 1017–1044 (1953).
5. H. Ogasawara, Theory for two-phase critical flow (5th report, several problems on orifice flow of saturated liquid), *Trans. JSME Series* 2, **34**(268), 2146–2154 (1968) [in Japanese].
6. M. Fujii, T. Watanabe, H. Nakamura and Y. Kukita, Two-phase discharge rate through a sharp-edged thin-plate orifice, *Proceedings of the 1st JSME/ASME Joint International Conference on Nuclear Engineering*, Vol. 1, Tokyo, pp. 203–209 (1991).
7. R. E. Henry and H. K. Fauske, The two-phase critical flow of one component mixtures in nozzles, *ASME J. Heat Transfer* **93**(5), 179–186 (1971).
8. M. A. Grolmes and J. C. Leung, Scaling considerations for two-phase critical flow, *Multi-Phase Flow and Heat Transfer III. Part A*, pp. 549–565. Elsevier Science Publishers B.V., Amsterdam (1984).
9. M. Epstein, R. E. Henry, W. Midvidy and R. Pauls, One-dimensional modeling of two-phase jet expansion and impingement, *Proceedings of the 2nd International Topical Meeting of Nuclear Reactor Thermal Hydraulics*, Santa Barbara, CA, Vol. 2, pp. 769–777 (1983).
10. J. C. Leung and M. A. Grolmes, A generalized correlation for flashing choked flow of initially subcooled liquid, *A.I.Ch.E. Jl* **34**(4), 688–691 (1988).
11. D. W. Sallet, Subcooled and saturated liquid flow through valves and nozzles, *J. Hazardous Mater.* **25,** 181–191 (1990).
12. R. K. Young and R. L. Hummel, Improved nucleate boiling heat transfer, *Chem. Engng Prog.* **60**(7), 53–58 (1964).
13. M. Isono, Two-phase critical flow at flow contraction by disk, M.S. Thesis, Tokyo University of Mercantile Marine (1995) [in Japanese].